CODED EXCITATION ULTRASOUND: EFFICIENT IMPLEMENTATION VIA FREQUENCY DOMAIN PROCESSING

Almog Lahav, Yuval Ben-Shalom, Tanya Chernyakova and Yonina C. Eldar

Technion - Israel Institute of Technology
Dept. of Electrical Engineering
Haifa 32000, Israel

ABSTRACT

Modern imaging systems use single-carrier short pulses for transducer excitation. The usage of coded signals allowing for pulse compression is known to improve signal-to-noise ratio (SNR), for example in radar and communication. One of the main challenges in applying coded excitation (CE) to medical imaging is frequency dependent attenuation in biological tissues. Previous work overcame this challenge and verified significant improvement in SNR and imaging depth by using an array of transducer elements and applying pulse compression at each element. However, this approach results in a large computational load. A common way of reducing the cost is to apply pulse compression after beamforming, which reduces image quality. In this work we propose a high-quality low cost method for CE imaging by integrating pulse compression into the recently developed frequency do- main beamforming framework. This approach yields a 26-fold reduction in computational complexity without compromising image quality. This reduction enables efficient implementation of CE in array imaging paving the way to enhanced SNR, improved imaging depth and higher frame-rate.

Index Terms— Array processing, coded excitation, beamforming, ultrasound.

1. INTRODUCTION

In standard ultrasound imaging, a transducer transmits a short single-carrier Gaussian pulse of acoustic energy into the tissue along a narrow beam. The echoes are scattered by the objects within the tissue and are detected by the transducer elements. These echoes, that are essentially the replicas of the transmitted pulse, are processed and presented as an image line. Consequently the axial resolution is defined by the duration of the transmitted pulse. Signal-to-noise ratio (SNR) and imaging depth can be improved by increasing the transmitted energy. However, transmitting more energy with the same pulse duration, i.e. resolution, requires higher peak intensity levels, which can potentially damage the tissue and thus are limited by the Food and Drug Administration (FDA).

When coded signals are used for excitation, pulse compression is performed on the detected signal by applying a matched filter (MF) defined by the transmitted pulse-shape. As a result a stream of pulse's replicas is converted to a stream of its autocorrelations. The width of the pulse's autocorrelation is on the order of the inverse bandwidth [1], implying that the resolution is now defined by the available system's bandwidth and is independent on pulse duration. Therefore, we can use a longer pulse and transmit more energy without degrading range resolution. Experimental results reported in [2] show improvement of 15-20 dB in SNR as well as 30-40 mm improvement in penetration depth obtained with coded excitation (CE). Beyond the improvement in imaging depth, high SNR allows the utilization of higher frequencies and consequently better image resolution. In addition, Misaridis and Jensen have shown a way to increase the frame rate by an orthogonal coding approach [3, 4, 5].

One of the main challenges of CE in medical ultrasound is its application to array imaging. Most modern imaging systems use multiple transducer elements to transmit and receive acoustic energy. This allows to perform beamforming during both transmission and reception. Dynamic beamforming upon reception results in optimal focusing at each depth and leads to SNR enhancement and improvement of angular localization. An ideal implementation of CE in array imaging requires a MF for every transducer element and thus results in high computational complexity. Most reported studies use either a single transducer element [4] or an array of transducer elements with one MF applied on the beamformed signal [2, 6]. The latter approach results in error in pulse compression and degrades image quality. This effect depends on the length of the transmitted pulse, the position of the transmit focus and imaging depth [2, 7].

In this work, we propose a solution for the computational complexity problem based on frequency domain beamforming. As shown in [8] beamforming can be performed equivalently in the frequency domain. By integrating the pulse compression into frequency domain beamforming, we apply a MF at each detected signal without affecting the complexity of frequency domain processing. For typical imaging parameters, the above approach leads to a 26 fold reduction in the number of multiplications compared to time domain implementation. This efficient implementation allows CE to become a practical approach in array imaging.

The rest of the paper is organized as follows: Section 2 briefly reviews basics of CE applied to medical imaging. In Section 3 we discuss the requirements and challenges of CE in the context of array imaging. We next propose a solution based on frequency domain beamforming in Section 4. Simulation results are presented in Section 5.

2. CODED EXCITATION IN MEDICAL ULTRASOUND

In CE a modulated signal is used for transducer excitation:

$$s(t) = a(t)\cos\left(2\pi f_0 t + \psi(t)\right), \tag{1}$$

where $\psi(t)$ and $a(t)$ are phase and amplitude modulation functions respectively, and f_0 is the central frequency of a transducer. Pulse compression is performed on the detected signal, $\varphi(t)$, by applying a MF, $h(t) = s^*(-t)$. For a signal comprised of K scatterers the output of the MF is a combination of autocorrelations of the transmitted pulse [3]:

$$\varphi^{CE}(t) = \varphi(t) * s^*(-t) = \sum_{k=1}^{K} \alpha_k R_{ss}(t - t_k), \tag{2}$$

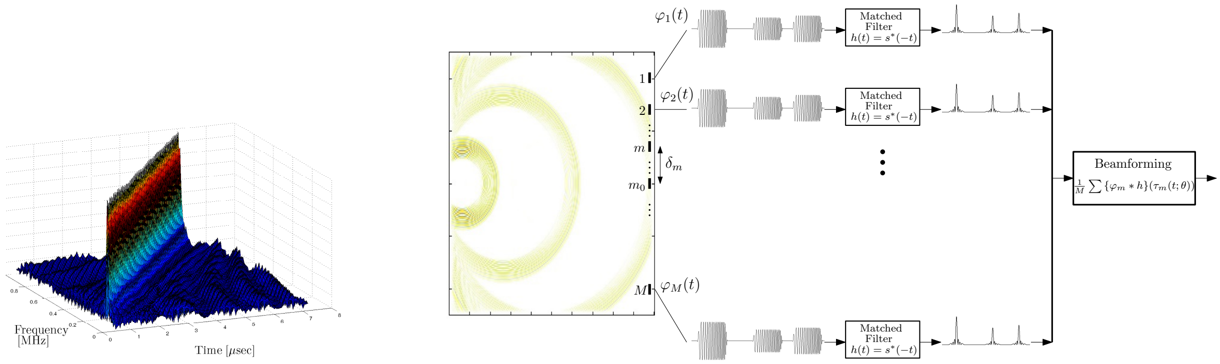

(a) (b)

Fig. 1. (a) Ambiguity function of Linear FM with time-bandwidth product of $D = 70$. (b) On the left echoes are reflected from 3 point scatterers in the medium. The received signal of each element is composed of reflections of a linear FM waveform. Beamforming is applied on compressed signals, obtained at the output of the MF.

where α_k and t_k denote the amplitude and the time delay of the reflection from the kth scatterer respectively. The half-power width of the main lobe of the autocorrelation, which determines the range resolution, is approximately equal to the inverse bandwidth B^{-1} of the transmitted pulse [1]. As a result, in contrast to conventional imaging, the pulse time duration, T , can be increased allowing for more transmit energy without degrading range resolution. The resulting gain in signal-to-nosie ratio (GSNR) of the MF processing is approximately equal to the time-bandwidth product TB [9].

The above result holds when the detected signal is comprised of the exact replicas of the transmitted pulse. In practice when acoustic wave propagates in biological tissues, high frequencies undergo stronger attenuation due to the medium properties. A common way to model this effect is to assume that it does not distort the complex envelope of the signal but only downshifts the central frequency [10]. This shift can be treated as a doppler shift. Therefore, in an attenuating medium the output of the MF is a stream of cross-sections of the ambiguity function of the transmitted pulse [3]:

$$\varphi^{CE}(t) = \varphi(t) * s^*(-t) = \sum_{k=1}^{K} \alpha_k A(t - t_k, f_k). \qquad (3)$$

The ambiguity function, $A(t-t_k, f_k)$, describes the MF output when the input signal has a frequency shift f_k and is delayed by t_k. In ultrasound imaging the frequency shifts do not carry valuable information and thus do not need to be found explicitly. Therefore, the ideal ambiguity function should have a good range resolution for all frequency shifts, while good frequency resolution is not required [3]. This makes linear frequency modulation (FM) a good choice for ultrasound imaging. For this choice:

$$s(t) = a(t)\cos\left(2\pi\left(f_0 t + \frac{B}{2T}t^2\right)\right), \quad -\frac{T}{2} \le t \le \frac{T}{2}. \qquad (4)$$

The frequency spectrum of a linear FM complex envelope is rectangular, so that the envelope of the MF output is approximately a sinc function [11]. One can recognize this shape in the cross sections of the linear FM ambiguity function shown in Fig. 1 parallel to the frequency axis. Note that these cross sections preserve their range resolution for every frequency shift, implying robustness to attenuation. Significant improvement of penetration depth and contrast obtained with linear FM excitation are reported in [4]. The results in [4] were obtained with a single-element transducer, while imaging systems today use an array of transducer elements. The implication of array processing is discussed next.

3. USE OF CODED EXCITATION IN ARRAY IMAGING

3.1. Dynamic Beamforming in Time

In ultrasound imaging a scan-line is obtained by beamforming, namely, averaging the detected signals after their alignment with appropriate time-dependent delays. In this way optimal focusing at each depth is obtained leading to SNR enhancement and improvement of angular localization. To derive an the beamforming equation we consider an array of M elements, illustrated in Fig. 1. Denote by m_0 the reference element and by δ_m its distance to the mth element, and by c the speed of sound. For a pulse transmitted in direction θ, the beamformed signal is given by [8]:

$$\Phi(t;\theta) = \frac{1}{M}\sum_{m=1}^{M} \varphi_m(\tau_m(t;\theta)) \qquad (5)$$
$$\tau_m(t;\theta) = \frac{1}{2}\left(t + \sqrt{t^2 - 4(\delta_m/c)t\sin\theta + 4(\delta_m/c)^2}\right),$$

where $\varphi_m(t)$ is the signal detected by the mth element and $\tau_m(t;\theta)$ is the time delay needed to be applied in order to align the reflection received by this element.

3.2. Matched Filtering and Beamforming

As explained in Section 2, in the CE approach, pulse compression is achieved by applying a MF on the detected signal. Array imaging requires matched filtering of the detected signal of every transducer element prior to beamforming as illustrated in Fig. 1. Using (5) and substituting the MF impulse response $h(t) = s^*(-t)$ the beamformed signal is given by:

$$\Phi_{CE}(t;\theta) = \frac{1}{M}\sum_{m=1}^{M} \{\varphi_m * h\}(\tau_m(t;\theta)). \qquad (6)$$

The practical meaning of this direct implementation is that the computational complexity is vastly increased by filtering each detected signal, which restricts the use of CE in array imaging. A trivial way to overcome this problem is beamforming pre-compression, i.e. beamforming is performed before pulse compression [7]. This requires only one MF allowing to save:

$$N \approx (N_e - 1)\left(\frac{3}{2}(N_s + N_h)\log(N_s + N_h) + N_s + N_h\right), \quad (7)$$

multiplications, where N_e, N_s and N_h are the number of elements, number of samples and MF length respectively. With this approach, however, we get a different expression for the resulting beamformed signal:

$$\Phi_{CE_{pre}}(t;\theta) = \left\{ \frac{1}{M} \sum_{m=1}^{M} \varphi_m(\tau_m(t;\theta)) \right\} * h(t). \quad (8)$$

As can be seen in (5), the applied delays are non-linear functions of time, which distort the phases of the coded signal. Therefore when preceding the compression, the delays result in an error in the compression:

$$e(t) = |\Phi_{CE}(t;\theta) - \Phi_{CE_{pre}}(t;\theta)|. \quad (9)$$

The error is larger for small depth and can be decreased by limiting pulse duration $T < 64/f_0$ [2, 7]. However this upper bound restricts the GSNR of the MF processing which is defined by the time-bandwidth product.

Fig. 2 shows a simulated scan-line with a point scatterer located at 25 mm from a transducer. The main lobe of the resulting point spread function is approximately 10% wider when beamforming is performed prior to pulse compression. In addition, the first side lobe from the left is 14 dB higher. Details on the simulation environment are elaborated in Section 5. Obviously when the trivial solution of beamforming pre-compression is used in order to reduce the computational complexity the image quality is compromised.

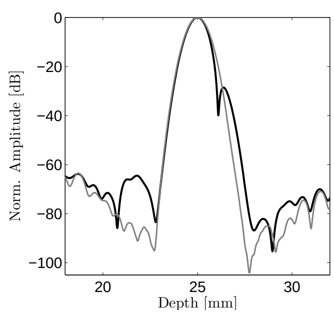

Fig. 2. A single scan-line of a point scatterer. The black line is produced with beamforming pre-compression, and the gray line is produced with beamforming post-compression.

4. INTEGRATING PULSE COMPRESSION IN FREQUENCY DOMAIN BEAMFORMING

As shown in [8] the beamforming can be performed equivalently in the frequency domain. In this section we will use the derivation in [12], and with appropriate changes obtain a new formulation of frequency domain beamforming that includes pulse compression at each element without increasing the computational complexity of this technique.

Let $\hat{\varphi}_m(t;\theta)$ be the signal received by the mth element after applying the beamforming delay:

$$\hat{\varphi}_m(t;\theta) = \varphi_m(\tau_m(t;\theta)). \quad (10)$$

Using (5) the Fourier series coefficients of the beamformed signal $\Phi(t;\theta)$ with respect to the interval $[0,T)$ can be expressed as [8]:

$$c[k] = \frac{1}{M} \sum_{m=1}^{M} \hat{c}_m[k], \quad (11)$$

where $\hat{c}_m[k]$ are given by:

$$\hat{c}_m[k] = \frac{1}{T} \int_0^T \varphi_m(t) q_{k,m}(t;\theta) e^{-i\frac{2\pi}{T}kt} dt. \quad (12)$$

The delays of every signal $\varphi_m(t)$ are effectively applied through the distortion function $q_{k,m}(t;\theta)$ defined in [8].

To incorporate pulse compression, each signal $\varphi_m(t)$ is replaced by the MF output:

$$\varphi_m^{CE}(t) = \{\varphi_m * h\}(t). \quad (13)$$

We next replace $\varphi_m^{CE}(t)$ by its Fourier coefficients $c_m^{CE}[n]$:

$$\begin{aligned} \hat{c}_m^{CE}[k] &= \frac{1}{T} \int_0^T \{\varphi_m * h\}(t) q_{k,m}(t;\theta) e^{-i\frac{2\pi}{T}kt} dt \quad (14) \\ &= \sum_n c_m^{CE}[n] \frac{1}{T} \int_0^T q_{k,m}(t;\theta) e^{-i\frac{2\pi}{T}(k-n)t} dt \\ &= \sum_n c_m^{CE}[k-n] Q_{k,m;\theta}[n], \end{aligned}$$

where $Q_{k,m;\theta}[n]$ are the Fourier coefficients of $q_{k,m}(t;\theta)$ with respect to $[0,T)$. When substituted by its Fourier coefficients, the distortion function effectively transfers the beamforming delays defined in (5) to the frequency domain. The function $q_{k,m}(t;\theta)$ depends only on the array geometry and is independent of the detected signals. Its Fourier coefficients can be computed off-line and used as a look-up-table (LUT) during the imaging cycle.

According to [8] most of the energy of the set $\{Q_{k,m;\theta}[n]\}$ is concentrated around the direct current (DC) component. This behavior is typical to any choice of k, m or θ. We therefore rewrite (14) as

$$\hat{c}_m^{CE}[k] \simeq \sum_{n=-N_1}^{N_2} c_m^{CE}[k-n] Q_{k,m;\theta}[n] \quad (15)$$

where the choice of N_1 and N_2 controls the approximation quality. According to (13) and the convolution theorem, the Fourier coefficients $c_m^{CE}[n]$ are given by $c_m[n]h[n]$, where $c_m[n]$ and $h[n]$ are the Fourier coefficients of the signal $\varphi_m(t)$ and the MF respectively. We can now rewrite (15) as

$$\begin{aligned} \hat{c}_m^{CE}[k] &\simeq \sum_{n=-N_1}^{N_2} c_m[k-n] h[k-n] Q_{k,m;\theta}[n] \quad (16) \\ &= \sum_{n=-N_1}^{N_2} c_m[k-n] \tilde{Q}_{k,m;\theta}[n] \end{aligned}$$

where the set $\{\tilde{Q}_{k,m;\theta}[n]\}$ includes the Fourier series coefficients of the MF and therefore performs beamforming and pulse compression simultaneously in the frequency domain. Obviously, incorporation of pulse compression does not affect computational complexity of frequency domain beamforming, since it only requires to update the set of frequency weights which is performed off-line. Substitution of (16) into (11) yields a relationship between the Fourier coefficients of the beam and the individual detected signals:

$$c[k] \simeq \frac{1}{M} \sum_{m=1}^{M} \sum_{n=-N_1}^{N_2} c_m[k-n] \tilde{Q}_{k,m;\theta}[n]. \quad (17)$$

Applying an inverse Fourier transform on $\{c[k]\}$ results in the beamformed signal in time.

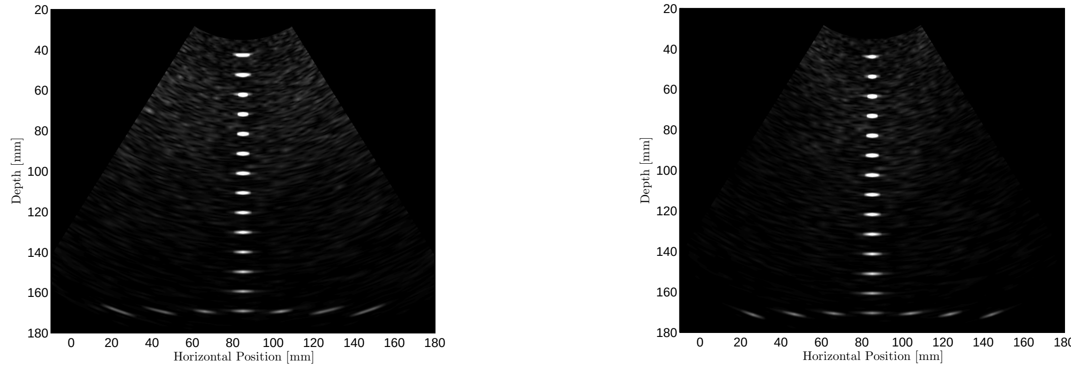

(a) (b)

Fig. 3. A medium with point scatterers every 10 mm on the range axis and horizontally in the depth of 170 mm. (a) Time domain processing. (b) Frequency domain processing.

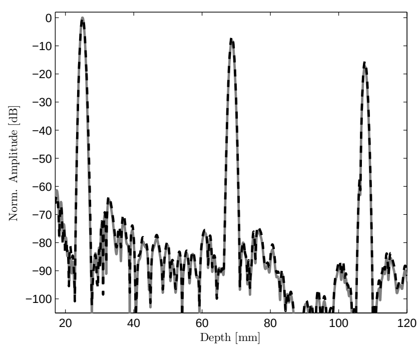

Fig. 4. A single scan-line of point scatterers positioned at 25, 70 and 110 mm. The black dashed and grey lines correspond to frequency domain beamforming with MF and time domain beamforming post-compression respectively.

5. RESULTS

To verify the performance of pulse compression in the frequency domain, we simulated CE imaging with an open source MATLAB toolbox: k-Wave [13]. The simulations run on the GPU card NVIDIA Tesla-K40 with 12Gb RAM, using MATLAB Parallel computing toolbox. Using k-Wave we simulated nonlinear ultrasound waves propagation in attenuating medium, corresponding to realistic tissue behavior [14]. High density point scatterers are positioned within the medium. The array contains 64 transducer elements, each one transmits a linear FM defined in (4), with time-bandwidth product $D = 100$, and central frequency $f_0 = 3.4$ MHz.

Fig. 4 compares two scan-lines of transmission at angle 0°, along the range axis. The black one is obtained by frequency domain beamforming with pulse compression according to (17), while the gray one results from applying a MF on every transducer element followed time domain beamforming. As can be seen, both methods yield identical results. In particular, we can see that around 25 mm the main lobe preserves its width and the side lobes are of the same amplitude, in contrast to beamforming pre-compression showed in Fig. 2. Two images with sector angle of 64° are presented in Fig. 3. Point scatterers are positioned on the range axis every 10 mm and horizontally in the depth of 170 mm. As can be seen, frequency domain beamforming achieves the same image quality as the time domain beamforming post-compression. The performances in terms of contrast and resolution are identical in both approaches.

For the derivation of the computational complexity reduction we consider only multiplications required in both methods. The number of samples comprising each scan-line is denoted by N_s, and is determined by the sampling rate. To avoid degradation of beam quality the rate should be 4-10 times the transducer's central frequency [15]. The Fourier coefficients of the beamformed signal given in (17) are a combination of the Fourier coefficients of the received signals $\varphi_m(t)$. The latter are obtained from the low-rate samples of the received signals, using the Xampling method [16, 17, 18] as elaborated in [8]. Hence, the number of multiplications needed for a computation of one scan-line using K coefficients from the set $\{c[k]\}$ is:

$$N_a = MKN_Q + \frac{N_s}{2}\log N_s, \tag{18}$$

including the inverse Fourier transform. Here N_Q denotes the number of $\tilde{Q}_{k,m;\theta}[n]$ coefficients taken for the approximation in (16).

When applying the conventional beamforming post-compression, the computation includes the complexity of M matched filters and interpolation of M signals to apply the time-varying delays. Assuming linear complexity for the linear interpolation and an efficient MF implementation using FFT:

$$N_b = MN_s + M\left(\frac{3(N_s+N_h)}{2}\log(N_s+N_h) + N_s + N_h\right), \tag{19}$$

multiplications are needed. For an array comprised of 64 elements and sampling rate $f_s = 16$ MHz the frequency domain beamforming requires 26 times less multiplications.

6. CONCLUSIONS

In this paper we proposed a method allowing to avoid the high computational load required by CE array imaging. The proposed method is based on integration of pulse compression applied to each one of the detected signals to the recently developed frequency domain processing scheme. Based on the comparison of single scan-lines and full images, we show that the above approach yields the same performances in terms of contrast and resolution while achieving 26 fold reduction in computational complexity. The achieved complexity reduction enables efficient implementation of CE in array imaging paving the way for enhanced SNR as well as improved imaging depth and frame-rate.

7. REFERENCES

[1] A. W. Rihaczek, *Principles of high-resolution radar*, McGraw-Hill New York, 1969.

[2] M. O'Donnell, "Coded excitation system for improving the penetration of real-time phased-array imaging systems," *Ultrasonics, Ferroelectrics, and Frequency Control, IEEE Transactions on*, vol. 39, no. 3, pp. 341–351, 1992.

[3] T. Misaridis and J. A. Jensen, "Use of modulated excitation signals in medical ultrasound. Part I: Basic concepts and expected benefits," *IEEE Transactions on Ultrasonics, Ferroelectrics and Frequency Control*, vol. 52, no. 2, pp. 177–191, 2005.

[4] T. Misaridis and J. A. Jensen, "Use of modulated excitation signals in medical ultrasound. Part II: Design and performance for medical imaging applications," *IEEE Transactions on Ultrasonics, Ferroelectrics and Frequency Control*, vol. 52, no. 2, pp. 192–207, 2005.

[5] T. Misaridis and J. A. Jensen, "Use of modulated excitation signals in medical ultrasound. Part III: high frame rate imaging," *IEEE Transactions on Ultrasonics, Ferroelectrics and Frequency Control*, vol. 52, no. 2, pp. 208–219, 2005.

[6] Y. Takeuchi, "An investigation of a spread energy method for medical ultrasound systems: Part one: Theory and investigation," *Ultrasonics*, vol. 17, no. 4, pp. 175–182, 1979.

[7] R. Bjerngaard and J. A. Jensen, "Should compression of coded waveforms be done before or after focusing?," in *Medical Imaging 2002*. International Society for Optics and Photonics, 2002, pp. 47–58.

[8] T. Chernyakova and Y. C. Eldar, "Fourier-domain beamforming: the path to compressed ultrasound imaging," *Ultrasonics, Ferroelectrics, and Frequency Control, IEEE Transactions on*, vol. 61, no. 8, pp. 1252–1267, 2014.

[9] D. R. Wehner, "High resolution radar (2nd)," *Edition. Artech House Inc*, 1995.

[10] J. A. Jensen, *Estimation of blood velocities using ultrasound: a signal processing approach*, Cambridge University Press, 1996.

[11] C.E. Cook and M. Bernfeld, "Radar signalsan introduction to theory and practice," 1967.

[12] N. Wagner, Y. C. Eldar, and Z. Friedman, "Compressed beamforming in ultrasound imaging," *IEEE Transactions on Signal Processing*, vol. 60, no. 9, pp. 4643–4657, 2012.

[13] B. E. Treeby and B. T. Cox, "k-wave: Matlab toolbox for the simulation and reconstruction of photoacoustic wave fields," *Journal of biomedical optics*, vol. 15, no. 2, pp. 021314–021314, 2010.

[14] B. E. Treeby, J. Jaros, A. P. Rendell, and B. T. Cox, "Modeling nonlinear ultrasound propagation in heterogeneous media with power law absorption using a k-space pseudospectral method," *The Journal of the Acoustical Society of America*, vol. 131, no. 6, pp. 4324–4336, 2012.

[15] B. D. Steinberg, "Digital beamforming in ultrasound," *IEEE Transactions on Ultrasonics, Ferroelectrics and Frequency Control*, vol. 39, no. 6, pp. 716–721, 1992.

[16] R. Tur, Y. C. Eldar, and Z. Friedman, "Innovation rate sampling of pulse streams with application to ultrasound imaging," *IEEE Transactions on Signal Processing*, vol. 59, no. 4, pp. 1827–1842, 2011.

[17] K. Gedalyahu, R. Tur, and Y. C. Eldar, "Multichannel sampling of pulse streams at the rate of innovation," *IEEE Transactions on Signal Processing*, vol. 59, no. 4, pp. 1491–1504, 2011.

[18] E. Baransky, G. Itzhak, I. Shmuel, N. Wagner, E. Shoshan, and Y. C. Eldar, "A sub-nyquist radar prototype: Hardware and algorithms," *IEEE Transactions on Aerospace and Electronic Systems, special issue on Compressed Sensing for Radar*, vol. 50, no. 2, pp. 809–822, 2014.